

# Recoil Properties of Fragments Formed in the 4.4 GeV Deuteron-Induced Reaction on Gold target

A. R. Balabekyan<sup>a</sup>, N. A. Demekhina<sup>b</sup>, G. S. Karapetyan<sup>c</sup>, L. Karayan<sup>a</sup>,  
J. R. Drnoyan<sup>d</sup>, V. I. Zhemelik<sup>d</sup>, J. Adam<sup>d</sup>, L. Zavorka<sup>d</sup>, A. A.  
Solnyshkin<sup>d</sup>, V. M. Tsouppko-Sitnikov<sup>d</sup>, J. Khushvaktov<sup>d</sup>, V. Guimarães<sup>c</sup>

*a) Yerevan State University, A. Manoogian,*

*1, 025, Yerevan, Armenia*

*b) Yerevan Physics Institute,*

*Alikhanyan Brothers 2,*

*Yerevan 0036, Armenia*

*c) Instituto de Fisica,*

*Universidade de Sao Paulo*

*Rua do Matao, Travessa R 187,*

*05508-900 S ao Paulo, SP, Brazil*

*d) Joint Institute for Nuclear Research (JINR),*

*Joliot-Curie 6, Dubna 141980,*

*Moscow region Russia*

## Abstract

The recoil properties of fragments produced by the interaction of 4.4 GeV deuteron with  $^{197}\text{Au}$  target have been studied. New experimental data on recoil properties for 90 nuclei, varying from  $^{24}\text{Na}$  to  $^{198}\text{Au}$ , were obtained. The technique applied was the *thick-target thick-catcher* and induced activity method. The deuteron beam was obtained from the Nuclotron of the Laboratory of High Energies (LHE), Joint Institute for Nuclear Research (JINR), Dubna. The experimental data were analyzed on the basis of the standard two-step vector model formalism. From this analysis we could find evidence to support the existence of several different mechanisms, such as spallation, fission and fragmentation, in the reaction investigated. Fission contributed appreciably to the formation of products in the mass region of  $65 \leq A \leq 120$ . The kinematic characteristics of residual nuclei formed in the present deuteron-induced reaction have been compared to those from proton-induced reactions with gold target.

PACS numbers: 25.45.-z, 25.60.Pj, 25.85.-w

## I. INTRODUCTION

In recent years, the interest to investigate kinematic characteristics of reaction products has been preconditioned by the attempt to create an universal picture of the interaction between high energy projectiles with heavy nuclei targets and to determine the basic mechanism responsible for the development of the several process that usually occur [1–3]. For instance, the possibility to obtain an unified presentation of the momentum and energy distributions of the fragments produced by interacting system would enrich the whole picture of reaction mechanism and would extend the conception of the reaction models. In relativistic nucleus-nucleus collisions, one of the most interesting question to be addressed is related to the energy transfer mechanism between the projectile and the target. Nuclear recoil experiments can provide valuable information, such as angular distributions and kinetic energies of the produced nuclei. These kind of information can deepen our understanding of the reaction mechanism and allows the test of different model representations.

Recoil properties of nuclei can be determined via the *thick-target thick-catcher* associated with the induced activity method. The *thick-target thick-catcher* method has been extensively applied to investigate hadron-induced reactions on various targets over a wide range of incident energy. The important feature in these experiments is that the thickness of the target and catcher foils should be larger than the longest range of the recoiled product. The quantities to be measured are the fractions of  $F$  and  $B$  intensities of the produced nuclides that recoil out of the target foil after the reaction into the catcher foils positioned at forward and backward directions, respectively. Such technique has been used to investigate the fragment kinematic properties of proton-induced reaction in uranium target [4, 5]. Also, for proton-nucleus on gold target, a wealth of data about the kinematic properties of fragments has been accumulated over the years [6–8]. These investigations were suitable to verify the contribution of different mechanisms such as fission, fragmentation, and spallation in the reaction. Moreover, experiments on kinematic properties for reaction induced by heavier projectiles, such as high-energy  $^{12}\text{C}$  ions, have also been performed, where target fragment angular distributions were obtained [9–11].

In the present paper we report the results for the recoil properties of the fragments produced by the interaction of 4.4 GeV deuteron with  $^{197}\text{Au}$  target. High energy reactions induced by deuteron have the particularity that, due to the low binding energy of the

deuteron (2.22 MeV), the reaction can proceed with the deuteron either as hole nucleus or as no interacting nucleons (proton plus neutron). These components are revealed in the present experiment by considering the analysis of the kinematics properties of the different mass region and compare with the results from proton-induced reaction at similar incident energies. We have also previously investigated recoil properties of fragments formed in the reactions induced by deuteron and proton beam at 3.65 GeV/nucleon on  $^{118}\text{Sn}$  target [12, 13]. We have used the same technique as in this work to measure the recoil properties of many of the same nuclides, thus permitting a comparison of how these properties vary with bombarding energy, target and projectile (single nucleon or system of composite nucleons).

The present paper is divided as follows; Section II is devoted to give some details on the experimental procedure and data analysis, where we have used the two-step vector model [14, 15]. In Section III we present the results and the discussion, where we have performed a comparison of the results with deuteron and proton induced reactions. Final conclusions is given in Section IV.

## II. EXPERIMENTAL PROCEDURE AND DATA ANALYSIS

The 4.4 GeV deuteron beam was obtained from the Nuclotron Laboratory of High Energies (LHE), Joint Institute for Nuclear Research (JINR), Dubna, and used to irradiate a  $39.13 \text{ mg/cm}^2$  thick gold target. The gold target consisted of a high-purity target metal foil of  $20 \times 20 \text{ mm}^2$ , and was sandwiched by a pair of  $7.0 \text{ mg/cm}^2$  thick Mylar foil with the same size (*catcher foils*). The Mylar foils were used to collect the nuclei that recoiled to the forward and backward directions with respect to the beam. To improve the statistics 15 gold target sandwiched by a pair of Mylar foil were piled up altogether. A solid angle of about  $2\pi$  is provided by using the catcher foils at the immediate vicinity of the target. The irradiation time was 28.6 hours with a total beam intensity of about  $(6.43 \pm 0.71) \cdot 10^{12}$  deuteron. The  $^{27}\text{Al}(d, 3p2n)^{24}\text{Na}$  reaction with the known cross sections of  $14.2 \pm 0.2 \text{ mb}$  [16] were used to monitor the beam. The  $\gamma$ -rays from the decay of the recoiled nuclides formed in the target and captured in the Mylar foils (*catcher foils*) were measured, in an off-line analysis, with High purity Germanium (HpGe) detector with 28% relative efficiency and an energy resolution of 2 keV ( $^{60}\text{Co}$  at 1332 keV). The measurements of  $\gamma$ -rays were performed over a period of time to follow the decay of the individual nuclide. The energy-dependent

detection efficiency of the HpGe detector was measured with standard calibration sources of  $^{54}\text{Mn}$ ,  $^{57;60}\text{Co}$ ,  $^{137}\text{Cs}$ ,  $^{154}\text{Eu}$ ,  $^{152}\text{Eu}$ , and  $^{133}\text{Ba}$ . The residual nuclides were identified by the energy, intensity of characteristic  $\gamma$ -lines, and by their respective half-lives. Nuclear properties, used to identify the observed isotopes, were taken from Ref. [17]. The half-lives of identified isotopes were within the range of 15 min and 1 yr. In the induced activity method used here, once we have obtained all the  $\gamma$ -ray, we could determine the production cross sections for each fragment and reaction products. In this particular experiment, where we used the *thick-target thick-catcher* method, we obtained the intensity fractions for each nuclide recoiled out of a target in the forward and backward direction, denoted  $F$  and  $B$ , respectively. The uncertainties in determining the intensity fraction for each radionuclide depended mainly on the following factors: the statistical significance of the yields ( $\leq 10\%$ ), the accuracy in measuring the target thickness and the accuracy of tabular data on nuclear constants ( $\leq 3\%$ ), and the errors in determining the detector energy-dependent efficiency ( $\leq 5\%$ ).

The measurements regarding the recoiling nuclei, such as the yields in the forward and backwards directions, were transformed into kinematic quantities by considering the two-step vector model [14, 15]. According to this method, the first stage of reaction involves the formation of the compound nucleus following by a cascade, leaving residual nucleus with an excitation energy  $E^*$  and a velocity  $\vec{v}$  (or the momentum  $\vec{p}$ ) along the beam direction. At the second stage, the residual nucleus evaporates nucleons and/or light particles, and as a result, the nucleus acquires an additional velocity  $\vec{V}$ . Thus, the velocity  $\vec{V}_i$  of a recoiling nuclide, in the laboratory system, is the sum of two vectors,  $\vec{V}_i = \vec{v} + \vec{V}$ . The velocity vector  $\vec{v}$  is the result of the fast projectile-target interaction, while the velocity vector  $\vec{V}$ , assumed to be isotropic in the moving system, is the result of the slow deexcitation of the excited primary fragment. The vector  $\vec{v}$  is assumed to be constant while the values of the vector  $\vec{V}$  are assumed to have a Maxwell distribution. It is also assumed that there is no correlation between the two vectors. Moreover, the vector  $\vec{v}$  can be decomposed into its two orthogonal components: parallel and perpendicular to the beam,  $v_{\parallel}$  and  $v_{\perp}$ , respectively. Also, according to the this two-step vector model it was assumed that there is no correlation between the velocity  $\vec{v}$  of the excited nucleus and  $\vec{V}$ , the angular distribution of fragments in the moving frame is isotropic, and  $v_{\perp}$  is zero.

The kinematic properties of the recoiling nuclides depend on their range inside the target

or catcher foils and their corresponding energy. It is convenient to express this relation as [14, 15]:

$$R = kV^N, \quad (1)$$

where  $R$  is the mean range (corresponding to  $V$ ),  $k$  and  $N$  are constants which can be evaluated from tables of ranges of nuclei recoiling into various materials [18].

As mentioned before, that main quantities measured in this experiment are the fractions of each nuclide recoiled out of the target in the forward or backward directions. These quantities are derived as;

$$F = S_F/(S_F + S_B + S_T), \quad B = S_B/(S_F + S_B + S_T), \quad (2)$$

where  $S_F$ ,  $S_B$ , and  $S_T$  are the yields associated with the products formed in the target, emitted in forward or backward directions, and absorbed by the corresponding catcher foil. These yields were then used to calculate the forward to backward ( $F/B$ ) anisotropy of the fragment emission and the ranges in the target material ( $R$ ).

The ranges and the  $F$  and  $B$  intensities are related by the following expression:

$$FW = \frac{1}{4}R[1 + \frac{2}{3}(N + 2)\eta + \frac{1}{4}(N + 1)^2\eta^2]; \quad BW = \frac{1}{4}R[1 - \frac{2}{3}(N + 2)\eta + \frac{1}{4}(N + 1)^2\eta^2] \quad (3)$$

where  $\eta = v/V$  ( $\eta_{\parallel} = v_{\parallel}/V$ , is the ratio of the parallel component of the first-step to the second-step velocity) and  $W$  is the target thickness in  $mg/cm^2$ .

The reaction product mean ranges ( $R$ ) were calculated using the follow expression [14, 15]:

$$R = 2W(F + B)/(1 + \frac{1}{4}(N + 1)^2\eta^2) \quad (4)$$

With the experimental values for the  $F$  and  $B$  and the mathematical formalism developed in the two-step vector model [14, 15], it was possible to calculate parameters that characterize the first ( $v_{\parallel}$ ,  $E^*$ ) and the second ( $R$  and  $T$ ) stages of the interaction, where  $T$  is the kinetic energy of a fragment and  $E^*$  is the mean excitation energy after cascade nucleus.

The relative velocity of the formed fragment,  $v_{\parallel}/v_{CN}$ , where  $v_{CN}$  is the velocity of a hypothetical compound nucleus formed in a complete fusion, is the main feature that can be considered as the sign of a complete or an incomplete fusion.

The value of the forward velocity  $v$  may be used to determine the average cascade deposition energy (excitation energy,  $E^*$ ) as follows: [19]:

$$E^* = 3.253 * 10^{-2} k' A_t v [T_p / (T_p + 2)]^{0.5}, \quad (5)$$

where  $E^*$  and the bombarding energy  $T_p$  are expressed in terms of  $m_p c^2$ .  $A_t$  is the target mass in  $amu$  and  $v$  is in units of  $(\text{MeV}/amu)^{0.5}$ . The constant  $k'$  has been evaluated by Scheidemann and Porile [19] on the basis of Monte Carlo cascade calculations as  $k' = 0.8$ .

### III. RESULTS AND DISCUSSION

The experimental values of  $F/B$  ratio are given in Table I for each nuclide observed in the present experiment. The  $F/B$  values represent somehow the extent of the recoiling nuclei at the forward direction, and thus can be considered an indirect measurement of the forward momentum transferred to the target nucleus in the reaction. The variation of  $F/B$  as a function of the product mass  $A$  is shown in Fig. 1. As it can be seen in this figure,  $F/B$  shows a peak at the high mass region which decreases as the mass loss from the compound nucleus increases, until about 20 nucleons have been lost. With further mass loss it goes to the deep spallation region (lower mass region). There is a broad minimum in the mass region of  $A = 45 - 75$ , and then  $F/B$  increases again as one goes to the light fragment region. A similar mass dependence has been observed previously for the 1-11.5 GeV proton bombardment on Au target [6]. This mass dependence could be explained by invoking different mechanisms for the production of nuclei in different mass regions. For high-energy induced reaction, as the case of the present experiment, heavy residual nuclei are produced mainly via spallation mechanism, with fragments preferably leaving at forward direction. On the other hand, the isotropic distribution of light nuclei may be due to fragmentation or fission-like processes.

The recoil parameter  $2W(F + B)$  is related to the mean ranges of the recoiling nuclei in the target material. Actually, the mean range of the recoils is somewhat smaller than  $2W(F + B)$ , but it is convention to refer to the latter as the range. The obtained values of this parameter for each nuclide studied in this experiment are listed in Table I and plotted as a function of the mass number  $A$  of the fragments in Fig. 2. A smooth curve has been

drawn over the data just to indicate the trend. The nuclides with higher mass, close to the mass of the compound system, is expected to be produced by the spallation process; and since it is a peripheral interaction, the values for the mean range,  $2W(F + B)$ , should be small, as observed. Intermediate mass range nuclides were formed mainly by deep spallation and fission-like mechanisms, and have a relatively larger range associated with a larger contribution of their binary decay. The particles with highest ranges are the light fragments  $^{24}\text{Na}$  and  $^{28}\text{Mg}$ . Such fragments can be produced, for instance, in (multi)fragmentation process with low impact parameter in the collision.

By analyzing the contents of Table I and II, some discussion about the different processes that can occur in the reaction of 4.4 GeV deuteron with gold can be made. The heaviest fragments ( $A \geq 131$ ) show large mean values of  $F/B \sim 3$  and very low fragment kinetic energies ( $\sim 0.03$  MeV/nucleon). These products are the result of spallation of the  $^{197}\text{Au}$  target. The products in the intermediate mass range of  $65 \leq A \leq 120$  have the average value of  $F/B = 1.64$  and mean kinetic energy of  $\sim 0.22$  MeV/nucleon. The lower  $F/B$  values obtained for these products in this mass range can be an evidence for fission process contribution. However, we can not clearly isolated the fission process contribution from the contribution of other processes (as deep spallation) in this mass range region. The lightest fragments,  $^{24}\text{Na}$  and  $^{28}\text{Mg}$  ( $A < 40$ ), are characterized by high kinetic energies and relatively large values of  $F/B$  and, thus, their production is consistent with a "multifragmentation" mechanism [20]. The intermediate mass fragments ( $40 < A < 65$ ) represent the group of fragments with relatively high kinetic energies ( $\sim 0.56$  MeV/nucleon) and large values of  $F/B = 1.50$ . Such fragments could be associate with fission where the heavy partner fragments would be in the mass region of  $A \sim 120 - 130$ . Deep spallation process may also contribute with products in this mass range. Deep spallation process can be responsible not only for the emission of nucleons and light charge particles (with  $Z \leq 2$ ) but also for emission of these relatively light fragments, specially if we take into account their high kinetic energies and formation in non peripheral collision (high values of  $F/B$ ).

The interesting question concerning the mechanism involved in relativistic nucleus-nucleus collision refers on how the energy transfer proceeds, whether the kinetic energy is transferred from the projectile to the target as a whole system or as energy per nucleon. To answer to this we compared our results of a deuteron induced reaction with those from reaction induced by high energy protons. In Figs. 3 and 4, we show such comparison for



recoil properties of fragments for the reaction induced by 4.4 GeV deuteron and similar measurements for the same products from the reaction induced by 1.0, 3.0 and 11.5 GeV protons with also  $^{197}\text{Au}$  target [6].

In Fig. 3 we present the comparison of the forward-to-backward ratio,  $F/B$ , for the deuteron and proton induced reactions at different energies. As mentioned before, nuclides at intermediate to high mass range are formed by spallation process which corresponds to a more peripheral collision. These heavier nuclides are formed with higher probability at lower projectile incident energies. Thus, by increasing the projectile energy, the spallation reaction probability decreases [21]. As can be observed in Fig. 3 (a), the ratio of  $F/B$  for 4.4 GeV deuteron and 1.0 GeV proton for the mass range of nuclides formed by deep spallation process are similar except for the spallation products (mass range of  $140 < A < 180$ ), where the  $(F/B)_{deuteron}/(F/B)_{proton}$  ratio drops off. The dropping of this ratio in this mass region is not observed in Figs. 3 (b) and (c) where the proton bombarding energy is higher, 3.0 GeV and 11.5 GeV, respectively. Actually, as the proton energy is further increased to 11.5 GeV, the  $(F/B)_{deuteron}/(F/B)_{proton}$  ratio are systematically larger. This can be explained by the domination of a non peripheral collisions with a smaller impact parameter for high-energy projectile. By observing the trend of the data in Fig. 3 (b), we can say that target fragment kinematic properties from deuteron-induced reaction mostly resemble those from the reaction induced by protons at the same total projectile energy. This observation is confirmed by theoretical calculations by Cugnon in Ref. [22] and it is consistent with the data of Kaufman [6], which found that the recoil properties of target fragment from reaction induced by 25.2 GeV  $^{12}\text{C}$  beam on  $^{197}\text{Au}$  are similar to those from the reaction induced by 28 GeV protons on  $^{197}\text{Au}$  target.

The other recoil property that can be used to compare the present data with those induced by protons at different incident energy is the recoil parameter,  $2W(F+B)$ , which is related to the mean range of the nuclides. Such comparison is presented in Figs. 4 (a), (b) and (c). As can be observed, the ratio of the values of  $2W(F+B)$  for products from both deuteron and proton induced reactions (especially the one at 3.0 GeV proton), as a function of the mass number are similar. This indicates that the deexcitation phase of these reactions is similar for this energy range.

A discussion on the transferred momentum and kinetic energy of the fragments can also be made. The two-step vector model applied here assumes that all the forward momentum

transferred from the incident particle occurs in the first step of the reaction ( $v_{\parallel}$ ), and all of the isotropic processes occur in the second step ( $V, T$ ), where the kinetic energy  $T$  is derived from range-energy data [18]. We listed in Table II the values of the kinetic energy ( $T$ ), the parameter  $N$ , as well as  $P(= AV)$  values for each nuclide, where  $P$  is the mean momentum imparted to the target fragment with mass number  $A$  during the deexcitation step of the reaction. The mean momentum  $P$  as a function of the mass number of the residual nuclides is present in Fig. 5. The dependence of  $P$  on the  $\Delta A^{0.5}$  (the square root of the number of nucleons removed from the target) is also indicated in this figure as the solid line curve. As one may observe (within certain broad limits) there is a general dependence of  $P$  upon  $\Delta A^{0.5}$ . The same tendency was found for the 8 GeV  $^{20}\text{Ne}$  with  $^{181}\text{Ta}$  system [23], which produces the same compound nucleus as the present work, and in the proton-induced reactions for the deep spallation product range  $A = 140 - 200$  [24]. According to the basic assumptions of the two-step vector model for high energy reactions, this dependence is an indication of a sequential, stepwise momentum kicks being imparted to the fragment during the deexcitation phase of the reaction. Also, the similarity of the  $P$  values for the fragments produced by different projectiles asserts that the deexcitation phase of these reactions is the same and does not depend on the type of projectile.

Due to correlation between  $v_{\parallel}$  and  $V$  we can estimate the parallel velocity component transferred to an intermediate nucleus in the first cascade step ( $v_{\parallel}$ ) and from the eq. (5) we can estimate the mean excitation energy of the residual nucleus after cascade nucleus ( $E^*$ ). The longitudinal velocity  $v_{\parallel}$  for the recoiling nuclei are presented in Table II and plotted in Fig. 6. The presence of a plateau at wide range of fragments can be explained as possible saturation of the energy-momentum transfer in a nuclear collision. For comparison, we also plotted in Fig. 6 the longitudinal velocity  $v_{\parallel}$  of the products from reactions induced by protons with 1.0, 3.0 and 11.5 GeV [6]. As we can observe in the figure, there is a gradual decrease of longitudinal velocity with the increase of the total projectile energy. Our data follow well the general tendency of  $v_{\parallel}$  values for protons. This behaviour suggests that a similar process takes place after the first step for reaction induced by different kind of incident particles at similar incident energy. This also may indicate a similar process for transferring the forward momentum. In summary, we can say that in the reactions induced by projectiles, with equivalent incident energy, on heavy targets, the first stage of the reaction and the deexcitation of the fragments following the initial fast stage, are carried out in a

similar manner.

The variation of excitation energy ( $E^*$ ) after cascade nucleus as a function of the mass number of fragments is shown in Fig. 7. For the medium-mass nuclides, the excitation energy is higher for the lighter nuclides, for example for  $^{24}\text{Na}$  and  $^{28}\text{Mg}$  nuclides (two outstanding points in the figure). Also, these nuclides requires the largest excitation energy for their formation mechanism. The residual nuclides in the mass range of  $65 \leq A \leq 120$  have about the same excitation energy, indicating that fission and probably deep spallation process take place at the same excitation energy regime. The products of spallation, the ones farther from the target mass, require more energy to be produced. The excitation energy for spallation products would be smaller if they were formed only by evaporation of light particles up to  $^4\text{He}$ . We divided the total mass range in regions and estimated, on the basis of eq. (5), the corresponding mean excitation energy. The obtained values consisted of  $1.416 \pm 283$  MeV (for the region of  $A < 40$ );  $472 \pm 95$  MeV (for  $42 \leq A \leq 59$ );  $353 \pm 71$  MeV (for  $65 \leq A \leq 120$ );  $264 \pm 53$  MeV (for  $A \geq 131$ ). This large variation of values can be understood by considering that different mechanism are involved in the formation of these residual nuclides [25–27].

#### IV. CONCLUSION

Kinematic properties of reaction products from the interaction of 4.4 GeV deuteron on  $^{197}\text{Au}$  target were investigated for the first time. The experimental results were analyzed on the basis of the two-step vector model and discussed in terms of different reaction mechanisms, such as spallation, fission, deep spallation and fragmentation.

The dependence of the recoil properties on the mass number of the product has been studied. The variation of the forward to backward intensity ratio,  $F/B$ , and mean recoil range,  $2W(F + B)$ , with the mass of the products show that heavier products were formed probably in a more peripheral collisions with large impact parameter, with relative low excitation energy, while medium and light mass products might have been produced in a more central collisions with smaller impact parameter and high excitation energy of the reaction remnant. The linear momentum transferred to an intermediate nucleus ( $p_{\parallel}$ ) shows a gradual decrease with the increase of the projectile energy. The combination of the information on the deposited energy,  $E^*$ , and on the forward cascade momentum allow us to suggest the existence of different mechanism in the formation of the products in this deuteron-induced

reaction.

The dependence of recoil properties on mass number of the product has been also compared to those from reactions induced by energetic protons on the same gold target. The similarity of the general picture of the mass dependence of the kinematic parameters concerning the first step (intranuclear cascade) and second (evaporation) stage is a clear indication that the interaction of protons and deuteron at the same energies are very similar. This behavior can be explained by the absence of additional interaction between the two nucleons of the deuteron with the target nucleus. This fact has been confirmed also by our previous work concerning the study of the cross sections of the deuteron and proton induced reactions on Sn isotopes [13].

## V. ACKNOWLEDGMENT

G. Karapetyan is grateful to Fundação de Amparo à Pesquisa do Estado de São Paulo (FAPESP) 2011/00314-0 and 2013/01754-9, and also to International Centre for Theoretical Physics (ICTP) under the Associate Grant Scheme. The authors are grateful to group leader of LNP JINR Dr. S. Avdeev for granting the possibility of carrying out this experiment, and also to the lead researcher of LHEP JINR Kh. Abraamyan for the help during the experiment.

- 
- [1] T. Enqvist, W. Wlazole, P. Armbruster *et al.*, Nucl. Phys. A **686**, 481 (2001).
  - [2] F. Rejmund, B. Mustapha, P. Armbruster *et al.*, Nucl. Phys. A **683**, 540 (2001).
  - [3] J. Taieb, K. H. Schmidt, L. Tassan-Got *et al.*, Nucl. Phys. A **724**, 413 (2003).
  - [4] K. Beg and N. T. Porile, Phys. Rev. C **3**, 1631 (1971).
  - [5] Y. W. Yu and N. T. Porile, Phys. Rev. C **8**, 1091 (1973).
  - [6] S. B. Kaufman, E. P. Steinberg, and M. W. Weisfield, Phys. Rev. C **18**, 1349 (1978).
  - [7] S. B. Kaufman and M. W. Weisfield, Phys. Rev. C **11**, 1258 (1975).
  - [8] M. Lagarde-Simonoff and G. N. Simonoff, Phys. Rev. C **20**, 1498 (1979).
  - [9] G. D. Cole and N. T. Porile, Phys. Rev. C **25**, 244 (1982).
  - [10] Y. Morita, W. Loveland, and G. T. Seaborg, Phys. Rev. C **28**, 2519 (1983).

- [11] Y. Morita, W. Loveland, P. L. McGaughey, and G. T. Seaborg, *Phys. Rev. C* **26**, 511 (1982).
- [12] A. R. Balabekyan, A. S. Danagulyan, J. R. Drnoyan, *et al.*, *Phys. At. Nucl.* **70**, 1892 (2007).
- [13] A. R. Balabekyan, A. S. Danagulyan, J. R. Drnoyan, *et al.*, *Phys. At. Nucl.* **69**, 1485 (2006).
- [14] L. Winsberg, *Phys. Rev. C* **22**, 2116 (1980) and *Phys. Rev. C* **22**, 2123 (1980).
- [15] L. Winsberg, *Nucl. Instrum. Methods* **150**, 465 (1978).
- [16] Ts. Damdinsuren, V.I. Iluschenko, P. Kozma, B. Tumendemberel, D. Chultem, *Yad. Fiz.* **52**, 330 (1990); [*Sov. J. Nuc. Phys.* **52**, 209 (1990)].
- [17] R. B. Firestone, in *Tables of Isotopes*, 8th ed.: 1998 Update (with CD ROM), edited by S. Y. Frank Chu (CD-ROM editor) and C. M. Baglin (Wiley Interscience, New York, 1996).
- [18] L. C. Northcliffe and R. E. Schilling, *Nucl. Data, Sect. A* **7**, 233 (1970).
- [19] O. Scheidemann and N. Porile, *Phys. Rev. C* **14**, 1534 (1976).
- [20] R. Wolfgang, E. W. Baker, A. A. Karetto *et al.*, *Phys. Rev.* **103**, 394 (1956).
- [21] S. B. Kaufman and E. P. Steinberg, *Phys. Rev. C* **22**, 167 (1980).
- [22] J. Cugnon, C. Volant, S. Vuillier, *Nucl. Phys. A* **625**, 729 (1997).
- [23] W. Loveland, D. J. Morrissey, K. Aleklett *et al.*, *Phys. Rev. C* **23**, 253 (1981).
- [24] V. P. Crespo, J. B. Cumming, and J. M. Alexander, *Phys. Rev. C* **2**, 1777 (1970).
- [25] K. Aleklett, W. Loveland, T. Lund, *et al.*, *Phys. Rev. C* **33**, 885 (1986).
- [26] N. Sugarman, M. Campos, K. Wielgoz, *Phys. Rev.* **101**, 388 (1956).
- [27] Y. W. Yu, C. H. Lee *et al.*, *Phys. Rev. C* **36**, 2396 (1987).

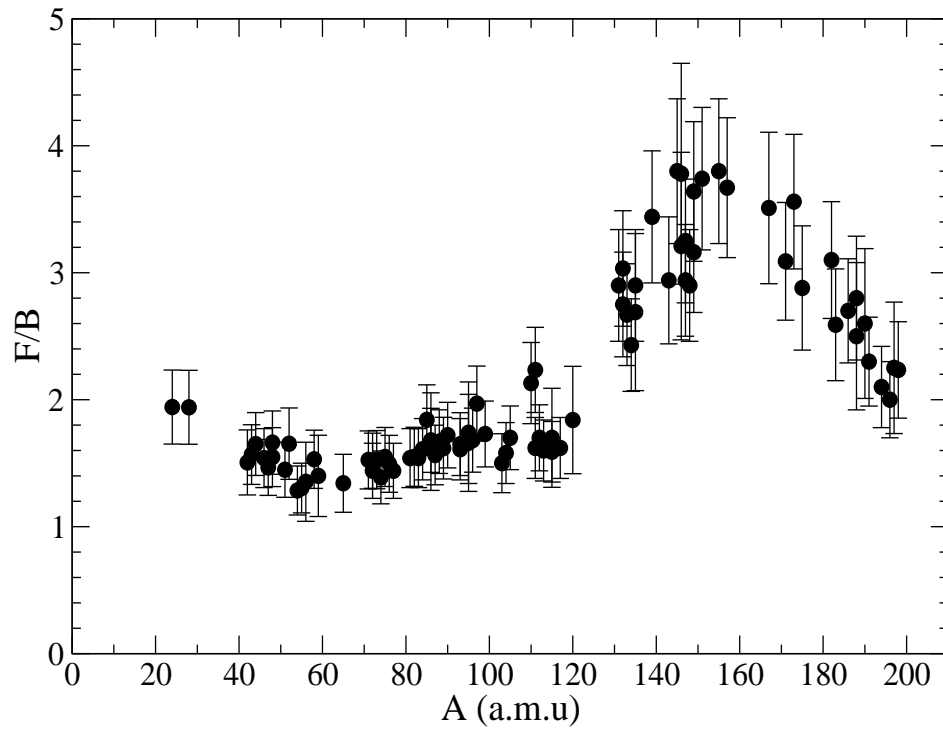


FIG. 1: Ratio of forward to backward intensities,  $F/B$ , as a function of the product mass number.

TABLE I: Target fragment recoil properties.  $W$  is the thickness of gold foil and thus  $2W(F + B)$  has unit of  $mg/cm^2$ .

Nuclide	$F/B$	$2W(F + B)$	Nuclide	$F/B$	$2W(F + B)$	Nuclide	$F/B$	$2W(F + B)$
$^{24}\text{Na}$	$1.94 \pm 0.29$	$15.7 \pm 2.3$	$^{86}\text{Rb}$	$1.67 \pm 0.38$	$5.1 \pm 1.1$	$^{135}\text{I}$	$2.69 \pm 0.61$	$1.52 \pm 0.35$
$^{28}\text{Mg}$	$1.94 \pm 0.29$	$14.5 \pm 2.1$	$^{86}\text{Y}$	$1.68 \pm 0.25$	$5.09 \pm 0.76$	$^{135}\text{Ce}$	$2.90 \pm 0.43$	$1.45 \pm 0.21$
$^{42}\text{K}$	$1.50 \pm 0.56$	$8.0 \pm 1.3$	$^{87}\text{Y}$	$1.56 \pm 0.23$	$5.59 \pm 0.83$	$^{139}\text{Ce}$	$3.44 \pm 0.51$	$1.41 \pm 0.21$
$^{43}\text{K}$	$1.57 \pm 0.23$	$7.9 \pm 1.1$	$^{88}\text{Y}$	$1.67 \pm 0.25$	$4.37 \pm 0.65$	$^{143}\text{Pm}$	$2.94 \pm 0.49$	$1.39 \pm 0.23$
$^{44m}\text{Sc}$	$1.65 \pm 0.25$	$7.2 \pm 1.0$	$^{89}\text{Zr}$	$1.61 \pm 0.24$	$5.01 \pm 0.75$	$^{145}\text{Eu}$	$3.80 \pm 0.57$	$1.26 \pm 0.18$
$^{46}\text{Sc}$	$1.54 \pm 0.23$	$8.3 \pm 1.2$	$^{90}\text{Nb}$	$1.72 \pm 0.25$	$4.57 \pm 0.68$	$^{146}\text{Eu}$	$3.78 \pm 0.86$	$1.37 \pm 0.31$
$^{47}\text{Ca}$	$1.47 \pm 0.22$	$8.2 \pm 1.2$	$^{93}\text{Mo}$	$1.65 \pm 0.24$	$3.97 \pm 0.59$	$^{146}\text{Gd}$	$3.21 \pm 0.73$	$1.46 \pm 0.33$
$^{48}\text{Sc}$	$1.66 \pm 0.25$	$8.2 \pm 1.2$	$^{93}\text{Tc}$	$1.60 \pm 0.24$	$4.02 \pm 0.60$	$^{147}\text{Eu}$	$2.94 \pm 0.44$	$1.43 \pm 0.21$
$^{48}\text{V}$	$1.55 \pm 0.23$	$7.0 \pm 1.0$	$^{95}\text{Zr}$	$1.66 \pm 0.38$	$4.03 \pm 0.92$	$^{147}\text{Gd}$	$3.25 \pm 0.48$	$1.38 \pm 0.20$
$^{51}\text{Cr}$	$1.44 \pm 0.22$	$7.4 \pm 1.1$	$^{95}\text{Nb}$	$1.74 \pm 0.40$	$4.8 \pm 1.1$	$^{148}\text{Eu}$	$2.90 \pm 0.43$	$1.33 \pm 0.19$
$^{52}\text{Mn}$	$1.65 \pm 0.28$	$5.9 \pm 1.0$	$^{96}\text{Tc}$	$1.68 \pm 0.25$	$4.66 \pm 0.69$	$^{149}\text{Eu}$	$3.16 \pm 0.47$	$1.15 \pm 0.17$
$^{54}\text{Mn}$	$1.28 \pm 0.19$	$7.5 \pm 1.1$	$^{97}\text{Ru}$	$1.96 \pm 0.29$	$4.50 \pm 0.67$	$^{149}\text{Gd}$	$3.64 \pm 0.54$	$1.19 \pm 0.17$
$^{55}\text{Co}$	$1.30 \pm 0.19$	$6.7 \pm 1.0$	$^{99}\text{Mo}$	$1.73 \pm 0.25$	$4.01 \pm 0.60$	$^{151}\text{Tb}$	$3.74 \pm 0.56$	$1.20 \pm 0.18$
$^{56}\text{Co}$	$1.35 \pm 0.31$	$7.1 \pm 1.6$	$^{103}\text{Ru}$	$1.50 \pm 0.22$	$5.59 \pm 0.83$	$^{155}\text{Dy}$	$3.80 \pm 0.57$	$1.16 \pm 0.17$
$^{58}\text{Co}$	$1.53 \pm 0.22$	$6.3 \pm 0.9$	$^{104}\text{Ag}$	$1.58 \pm 0.23$	$5.22 \pm 0.78$	$^{157}\text{Dy}$	$3.67 \pm 0.55$	$1.13 \pm 0.16$
$^{59}\text{Fe}$	$1.40 \pm 0.32$	$7.3 \pm 1.6$	$^{105}\text{Ag}$	$1.70 \pm 0.25$	$5.21 \pm 0.78$	$^{167}\text{Tm}$	$3.51 \pm 0.59$	$0.75 \pm 0.12$
$^{65}\text{Zn}$	$1.34 \pm 0.22$	$5.4 \pm 0.9$	$^{110}\text{In}$	$2.13 \pm 0.31$	$3.18 \pm 0.47$	$^{171}\text{Lu}$	$3.09 \pm 0.46$	$0.60 \pm 0.09$
$^{71}\text{As}$	$1.52 \pm 0.22$	$8.7 \pm 1.3$	$^{111}\text{Ag}$	$1.62 \pm 0.24$	$4.88 \pm 0.73$	$^{173}\text{Hf}$	$3.56 \pm 0.53$	$0.67 \pm 0.10$
$^{72}\text{Zn}$	$1.44 \pm 0.21$	$6.7 \pm 1.0$	$^{111}\text{In}$	$2.23 \pm 0.33$	$3.79 \pm 0.56$	$^{175}\text{Hf}$	$2.88 \pm 0.48$	$0.61 \pm 0.10$
$^{72}\text{As}$	$1.51 \pm 0.22$	$7.6 \pm 1.1$	$^{112}\text{Pd}$	$1.70 \pm 0.25$	$4.79 \pm 0.71$	$^{182}\text{Os}$	$3.10 \pm 0.46$	$0.44 \pm 0.06$
$^{73}\text{Se}$	$1.52 \pm 0.22$	$7.1 \pm 1.0$	$^{113}\text{Sn}$	$1.60 \pm 0.24$	$4.30 \pm 0.64$	$^{183}\text{Re}$	$2.59 \pm 0.44$	$0.51 \pm 0.08$
$^{74}\text{As}$	$1.38 \pm 0.20$	$7.3 \pm 1.1$	$^{115}\text{Ag}$	$1.70 \pm 0.39$	$4.14 \pm 0.95$	$^{186}\text{Ir}$	$2.70 \pm 0.40$	$0.23 \pm 0.03$
$^{75}\text{Se}$	$1.54 \pm 0.23$	$5.0 \pm 0.7$	$^{115m}\text{Cd}$	$1.59 \pm 0.23$	$4.62 \pm 0.69$	$^{188}\text{Ir}$	$2.50 \pm 0.57$	$0.22 \pm 0.05$
$^{76}\text{Br}$	$1.49 \pm 0.22$	$5.6 \pm 0.8$	$^{117m}\text{Sn}$	$1.62 \pm 0.24$	$3.77 \pm 0.56$	$^{188}\text{Pt}$	$2.80 \pm 0.47$	$0.23 \pm 0.03$
$^{77}\text{Br}$	$1.44 \pm 0.21$	$6.5 \pm 0.9$	$^{120m}\text{Sb}$	$1.84 \pm 0.42$	$3.00 \pm 0.69$	$^{190}\text{Ir}$	$2.60 \pm 0.59$	$0.20 \pm 0.04$
$^{81}\text{Rb}$	$1.54 \pm 0.23$	$6.4 \pm 0.9$	$^{131}\text{Ba}$	$2.90 \pm 0.43$	$2.90 \pm 0.43$	$^{191}\text{Pt}$	$2.30 \pm 0.34$	$0.19 \pm 0.02$
$^{82}\text{Br}$	$1.55 \pm 0.23$	$6.6 \pm 1.0$	$^{132}\text{Te}$	$3.033 \pm 0.45$	$2.00 \pm 0.30$	$^{194}\text{Au}$	$2.10 \pm 0.31$	$0.12 \pm 0.02$
$^{83}\text{Rb}$	$1.54 \pm 0.23$	$6.2 \pm 0.9$	$^{132}\text{Ce}$	$2.75 \pm 0.41$	$1.66 \pm 0.24$	$^{196}\text{Au}$	$2.00 \pm 0.30$	$0.07 \pm 0.01$

TABLE II: Target fragment kinematic properties as deduced from the two-step vector model. The kinetic energy  $T$  in unit of MeV, the momentum  $P$  is in unit of  $(MeV \cdot a.m.u.)^{1/2}$  and  $v_{\parallel}$  is in unit of  $(MeV/a.m.u.)^{1/2}$

Nuclide	$N$	$T$	$P[= AV]$	$v_{\parallel}$	Nuclide	$N$	$T$	$P[= AV]$	$v_{\parallel}$
$^{24}\text{Na}$	1.59	47.4±7.1	47.5±7.1	0.21±0.03	$^{86}\text{Rb}$	1.10	17±2	54±12	0.08±0.01
$^{28}\text{Mg}$	1.47	45.0±6.8	51.1±7.7	0.29±0.04	$^{86}\text{Y}$	1.20	18.7±2.8	56.1±8.1	0.08±0.01
$^{42}\text{K}$	1.15	27.0±4.0	47.6±8.0	0.12±0.02	$^{87}\text{Y}$	1.20	21.7±3.2	60.9±9.1	0.08±0.01
$^{43}\text{K}$	1.13	26.0±3.9	47.3±7.1	0.12±0.02	$^{88}\text{Y}$	1.20	14.2±2.1	49.3±7.3	0.07±0.01
$^{44m}\text{Sc}$	1.09	24.9±3.7	46.1±6.9	0.13±0.02	$^{89}\text{Zr}$	1.13	18.1±2.7	56.7±8.5	0.08±0.01
$^{46}\text{Sc}$	1.12	30.9±4.6	53.4±8.0	0.12±0.02	$^{90}\text{Nb}$	1.15	15.9±2.4	53.7±8.0	0.08±0.01
$^{47}\text{Ca}$	1.09	28.5±4.3	59.9±8.8	0.10±0.01	$^{93}\text{Mo}$	1.28	13.2±1.9	48.3±7.2	0.07±0.01
$^{48}\text{Sc}$	1.12	33.4±5.0	52.9±7.9	0.15±0.02	$^{93}\text{Tc}$	1.18	13.6±2.0	50.6±7.6	0.06±0.01
$^{48}\text{V}$	1.10	25.2±3.8	49.2±7.3	0.11±0.02	$^{95}\text{Zr}$	1.13	11.7±1.7	47.6±10.9	0.06±0.01
$^{51}\text{Cr}$	1.09	28.5±4.3	59.1±8.8	0.10±0.01	$^{95}\text{Nb}$	1.15	17.0±2.5	55.6±12.8	0.08±0.01
$^{52}\text{Mn}$	1.08	19.5±2.9	45.2±7.6	0.11±0.02	$^{96}\text{Tc}$	1.18	17.1±2.5	57.0±8.5	0.08±0.01
$^{54}\text{Mn}$	1.09	29.5±4.4	56.6±8.8	0.07±0.01	$^{97}\text{Ru}$	1.14	16.2±2.4	56.6±8.4	0.10±0.01
$^{55}\text{Co}$	1.08	26.5±4.0	54.1±8.1	0.07±0.01	$^{99}\text{Mo}$	1.28	13.0±1.9	49.6±7.4	0.07±0.01
$^{56}\text{Co}$	1.08	29.0±4.3	57.0±13.2	0.08±0.01	$^{103}\text{Ru}$	1.14	22.6±3.4	67.4±10.1	0.07±0.01
$^{58}\text{Co}$	1.07	22.3±3.3	50.9±7.6	0.09±0.01	$^{104}\text{Ag}$	1.24	22.2±3.3	67.1±10.0	0.07±0.01
$^{59}\text{Fe}$	1.07	27.4±4.1	57.1±13.1	0.08±0.01	$^{105}\text{Ag}$	1.24	22.0±3.3	67.0±10.0	0.08±0.01
$^{65}\text{Zn}$	1.11	17.7±2.6	43.7±7.4	0.05±0.01	$^{110}\text{In}$	1.21	10.1±1.5	49.1±7.3	0.08±0.01
$^{71}\text{As}$	1.06	45.4±6.8	75.5±11.3	0.11±0.02	$^{111}\text{Ag}$	1.24	19.1±2.8	63.8±9.5	0.07±0.01
$^{72}\text{Zn}$	1.08	23.7±3.5	58.2±7.7	0.07±0.01	$^{111}\text{In}$	1.21	13.4±2.0	55.7±8.3	0.10±0.01
$^{72}\text{As}$	1.06	36.4±5.4	67.6±10.1	0.10±0.02	$^{112}\text{Pd}$	1.24	17.9±2.6	61.7±9.2	0.07±0.01
$^{73}\text{Se}$	1.08	32.1±4.8	68.3±10.2	0.10±0.01	$^{113}\text{Sn}$	1.28	17.2±2.5	62.0±9.3	0.06±0.01
$^{74}\text{As}$	1.08	31.9±4.7	65.3±9.8	0.08±0.01	$^{115}\text{Ag}$	1.24	14.3±2.1	56.6±13.0	0.06±0.01
$^{75}\text{Se}$	1.12	31.3±4.6	49.6±7.4	0.10±0.01	$^{115m}\text{Cd}$	1.25	17.8±2.6	63.9±9.5	0.06±0.01
$^{76}\text{Br}$	1.08	21.1±3.1	55.8±8.3	0.07±0.01	$^{117m}\text{Sn}$	1.28	13.8±2.0	56.6±8.4	0.06±0.01
$^{77}\text{Br}$	1.08	26.6±3.9	63.8±9.5	0.08±0.01	$^{120m}\text{Sb}$	1.31	9.8±1.4	46.1±10.6	0.06±0.01
$^{81}\text{Rb}$	1.10	26.9±4.0	65.2±9.7	0.09±0.01	$^{131}\text{Ba}$	1.26	9.8±1.4	54.2±8.1	0.10±0.01
$^{82}\text{Br}$	1.08	26.4±3.9	65.6±9.8	0.09±0.01	$^{132}\text{Te}$	1.27	5.0±0.8	42.3±6.3	0.07±0.01
$^{83}\text{Rb}$	1.10	26.1±3.9	65.0±9.7	0.08±0.01	$^{132}\text{Ce}$	1.87	6.3±0.10	40.9±6.1	0.08±0.01



TABLE III: Continuation of Table II.

Nuclide	$N$	$T$	$P[= AV]$	$v_{\parallel}$	Nuclide	$N$	$T$	$P[= AV]$	$v_{\parallel}$
$^{135}\text{I}$	1.32	$3.54\pm 0.53$	$37.2\pm 8.5$	$0.05\pm 0.01$	$^{167}\text{Tm}$	2.02	$3.51\pm 0.59$	$34.2\pm 5.8$	$0.05\pm 0.01$
$^{135}\text{Ce}$	1.87	$5.51\pm 0.83$	$38.5\pm 5.7$	$0.07\pm 0.01$	$^{171}\text{Lu}$	2.07	$2.97\pm 0.44$	$31.8\pm 4.7$	$0.04\pm 0.01$
$^{139}\text{Ce}$	1.87	$5.30\pm 0.79$	$38.3\pm 5.7$	$0.08\pm 0.01$	$^{173}\text{Hf}$	2.05	$3.36\pm 0.50$	$31.7\pm 4.7$	$0.06\pm 0.01$
$^{143}\text{Pm}$	1.90	$5.53\pm 0.83$	$39.7\pm 6.7$	$0.07\pm 0.01$	$^{175}\text{Hf}$	2.05	$3.05\pm 0.46$	$30.5\pm 5.2$	$0.05\pm 0.01$
$^{145}\text{Eu}$	1.96	$5.25\pm 0.79$	$38.9\pm 5.8$	$0.09\pm 0.01$	$^{182}\text{Os}$	2.14	$2.42\pm 0.36$	$29.9\pm 4.4$	$0.04\pm 0.01$
$^{146}\text{Eu}$	1.96	$5.72\pm 0.86$	$42.0\pm 9.6$	$0.09\pm 0.01$	$^{183}\text{Re}$	2.19	$2.76\pm 0.41$	$32.2\pm 5.4$	$0.04\pm 0.01$
$^{146}\text{Gd}$	1.90	$6.25\pm 0.94$	$42.6\pm 9.8$	$0.08\pm 0.01$	$^{186}\text{Ir}$	2.13	$1.35\pm 0.20$	$22.7\pm 3.4$	$0.030\pm 0.004$
$^{147}\text{Eu}$	1.97	$5.97\pm 0.90$	$42.4\pm 6.3$	$0.07\pm 0.01$	$^{188}\text{Ir}$	2.13	$1.32\pm 0.20$	$22.5\pm 5.1$	$0.030\pm 0.004$
$^{147}\text{Gd}$	1.90	$5.89\pm 0.88$	$41.5\pm 6.2$	$0.08\pm 0.01$	$^{188}\text{Pt}$	2.14	$1.38\pm 0.21$	$23.1\pm 3.9$	$0.030\pm 0.004$
$^{148}\text{Eu}$	1.96	$5.55\pm 0.83$	$40.4\pm 6.0$	$0.07\pm 0.01$	$^{190}\text{Ir}$	2.13	$1.18\pm 0.18$	$21.5\pm 4.9$	$0.030\pm 0.004$
$^{149}\text{Eu}$	1.96	$4.78\pm 0.72$	$37.9\pm 5.6$	$0.07\pm 0.01$	$^{191}\text{Pt}$	2.14	$1.15\pm 0.17$	$27.3\pm 4.1$	$0.020\pm 0.003$
$^{149}\text{Gd}$	1.90	$5.03\pm 0.75$	$38.1\pm 5.7$	$0.08\pm 0.01$	$^{194}\text{Au}$	2.15	$0.81\pm 0.11$	$18.1\pm 2.7$	$0.020\pm 0.002$
$^{151}\text{Tb}$	1.94	$5.19\pm 0.78$	$39.0\pm 5.8$	$0.08\pm 0.01$	$^{196}\text{Au}$	2.15	$0.50\pm 0.07$	$14.0\pm 2.1$	$0.010\pm 0.002$
$^{155}\text{Dy}$	1.94	$5.18\pm 0.78$	$40.1\pm 6.0$	$0.08\pm 0.01$	$^{197m}\text{Hg}$	2.22	$0.76\pm 0.17$	$17.3\pm 3.8$	$0.020\pm 0.003$
$^{157}\text{Dy}$	1.95	$4.99\pm 0.75$	$39.6\pm 5.9$	$0.08\pm 0.01$	$^{198}\text{Au}$	2.15	$0.63\pm 0.09$	$15.6\pm 2.6$	$0.020\pm 0.002$

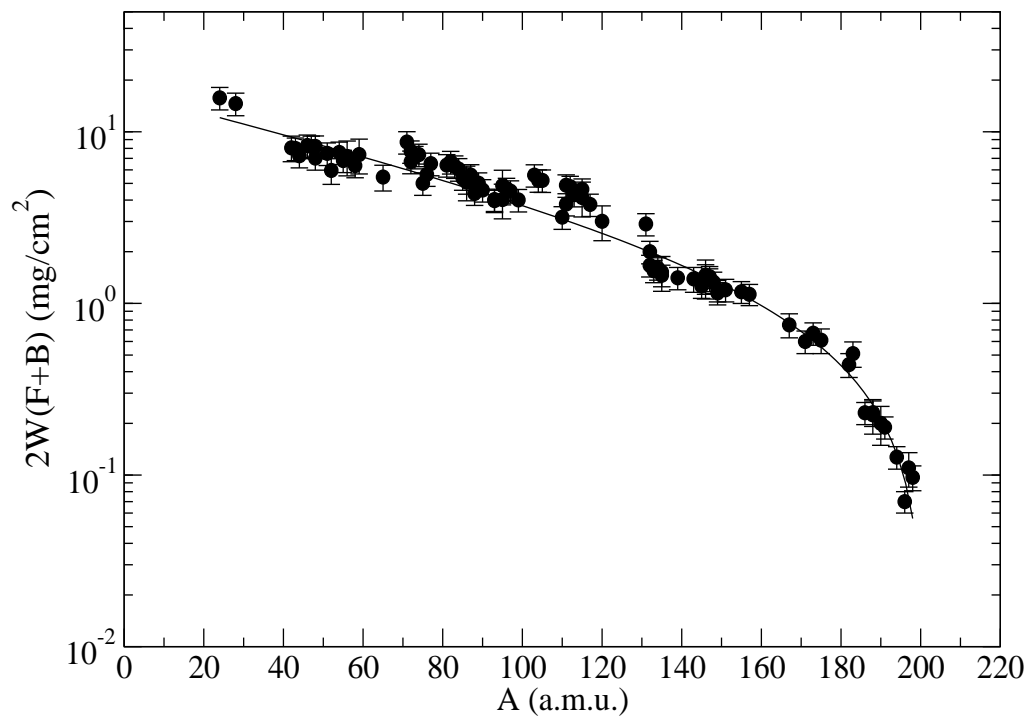


FIG. 2: The mean range,  $2W(F+B)$ , as a function of the product mass number. The curve shows the general trend of the data.

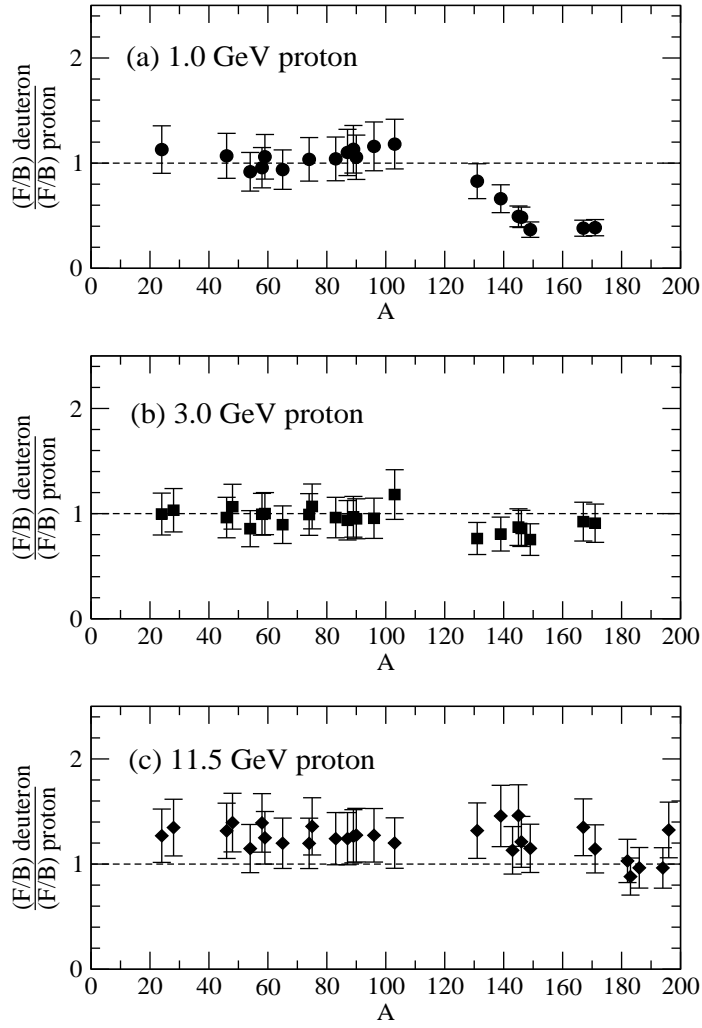


FIG. 3: The ratio of  $F/B$  values from the present work and those measured for the reaction induced by 1.0 GeV, 3.0 GeV and 11.5 GeV protons from Ref. [6], as indicated.

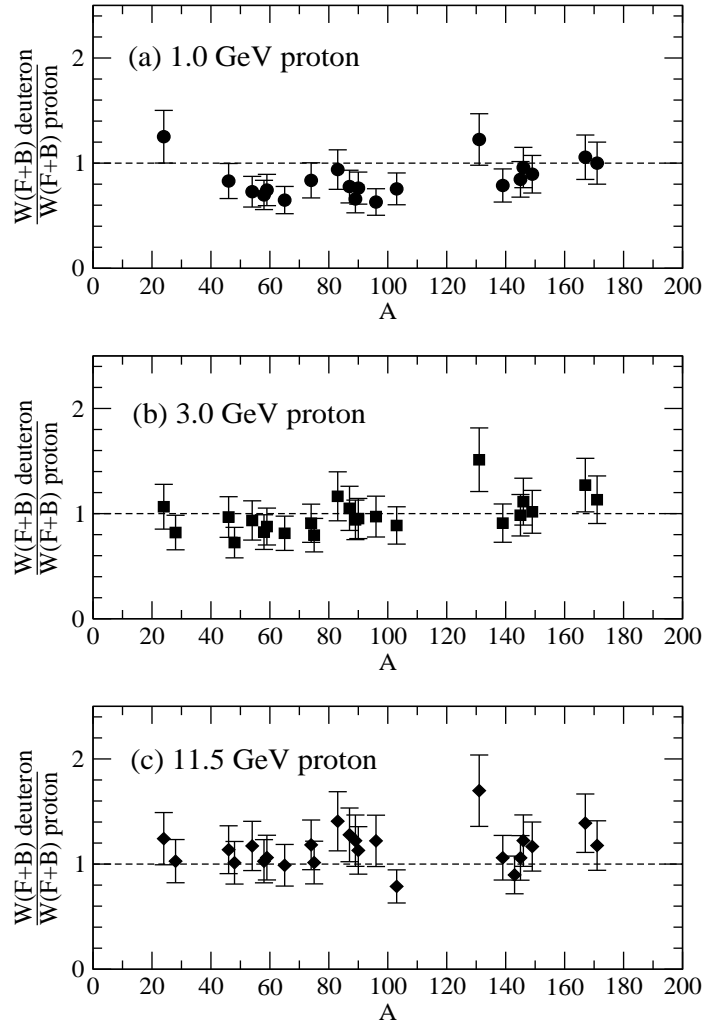


FIG. 4: The ratio of the  $2W(F + B)$  values from the present work and those measured for the reaction induced by 1.0 GeV, 3.0 GeV and 11.5 GeV protons from Ref. [6], as indicated, as a function of the target fragment mass.

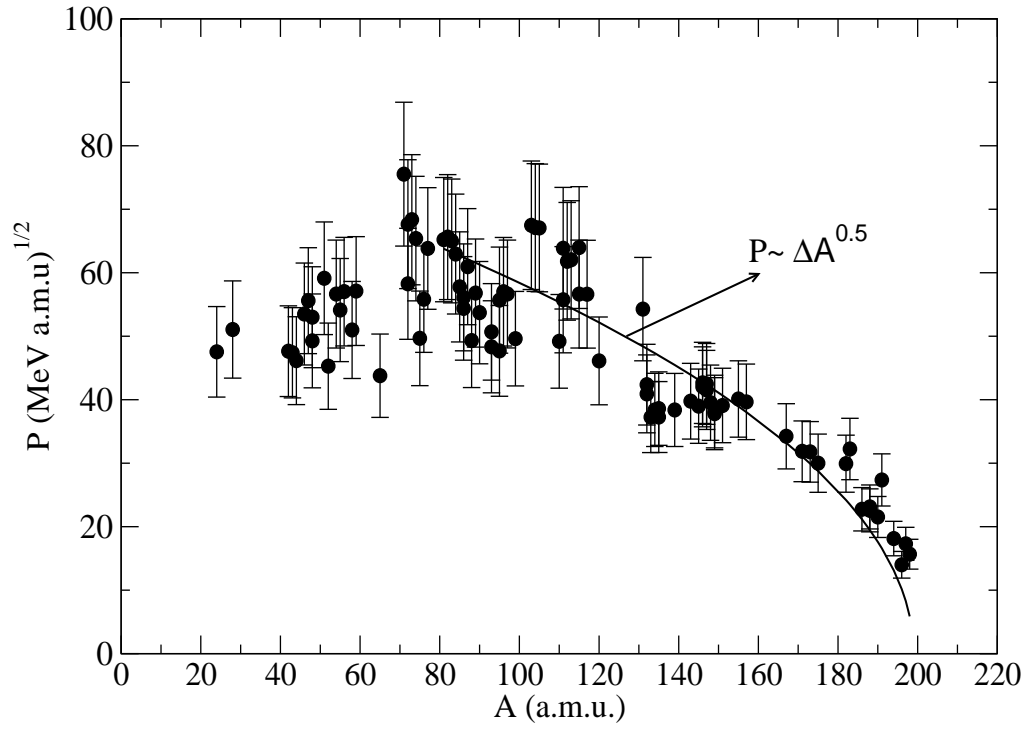


FIG. 5: The mean momentum,  $P = AV$ , as a function of product mass number. Solid line is  $P \sim \Delta A^{0.5}$  dependence.

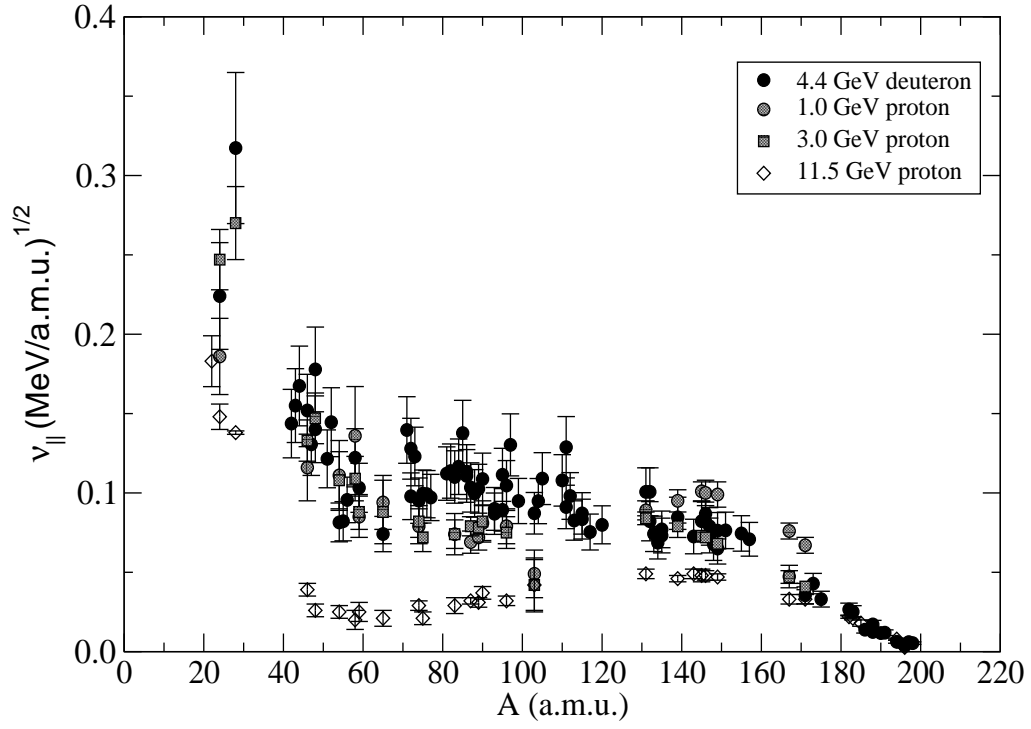


FIG. 6: The longitudinal velocity of residual nuclides after cascade nuclei,  $v_{||}$ , as a function of their mass number,  $A$ . The black circles are data from the present work. Gray and open symbols are data from proton-induced reaction on Au [6], with energies as indicated.

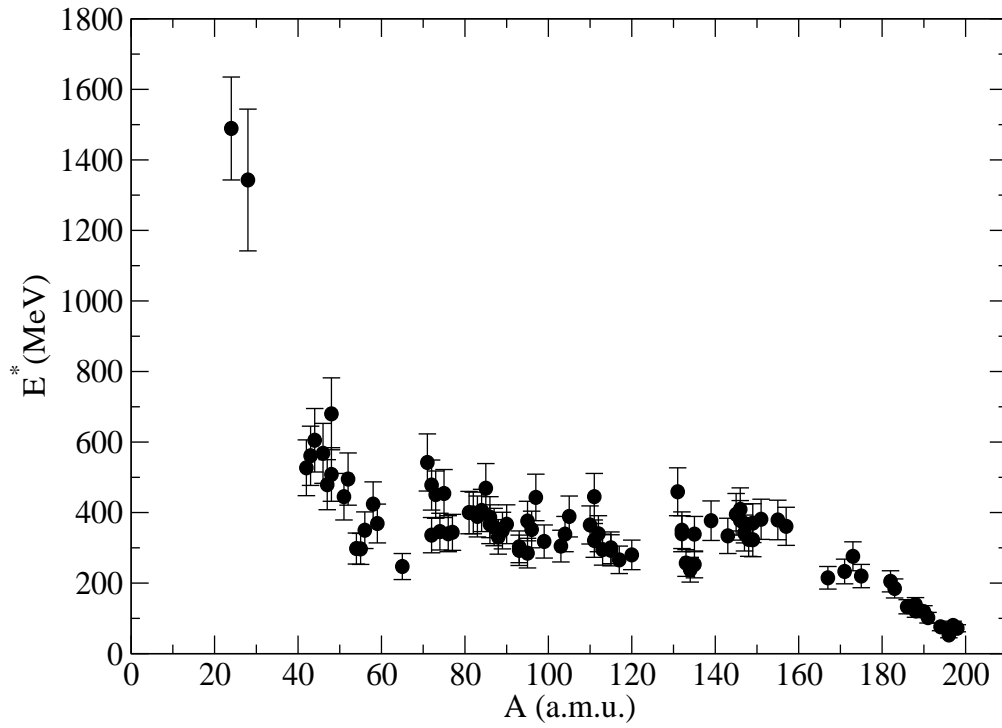


FIG. 7: Mean excitation energy of the residual cascade nucleus ( $E^*$ ) as a function of the product mass number.